Time-Resolved Light Scattering Studies on the Early Stage of Crystallization in Isotactic Polypropylene

Tetsuo Okada, Hiromu Saito, and Takashi Inoue*

Department of Organic and Polymeric Materials, Tokyo Institute of Technology, Ookayama, Meguro-ku, Tokyo 152, Japan

Received October 17, 1991

ABSTRACT: Crystallization kinetics in isotactic polypropylene was investigated by time-resolved light scattering under both H_V (cross-polarized) and V_V (parallel-polarized) optical alignments. Following an induction period, the density fluctuation started to increase, and then after a certain time lag, onset of the orientation fluctuation was observed, suggesting the development of an isotropic embryo at the early stage of crystallization. The growth of the embryo was found to follow the Avrami equation. Its radius linearly increased with time, and the temperature dependence of the linear growth rate was successfully interpreted by the Hoffman–Lauritzen theory. The embryo was estimated to be a highly disordered crystalline domain with low crystallinity.

Introduction

A spherulite is a crystal aggregate with spherical symmetry. Such aggregation arises by radial growth of a crystal from a common center. The spherulitic growth is believed to occur in two ways, as depicted in Figure 1.[1,2] In the growth mechanism A, a central nucleating entity initiates crystal growth in all directions. In the growth mechanism B, the spherulite develops from one single crystal through essentially unidirectional growth and the spherical shape is attained through continuous branching and fanning via the intermediate stage of sheaves.[2]

The above schemes have come mostly from microscopic observations by a polarized microscope and a transmission electron microscope (TEM). Polarized microscopy is usually informative on the morphology in a few microns to several tens of microns. TEM provides us morphology on different levels of the structural hierarchy, i.e., from the lamellar level to the spherulitic architecture. However, for TEM observation, one has to cool the specimen crystallized at a high crystallization temperature (T_c) down to room temperature to carry out the pretreatment, such as permanganic etching and RuO_4 staining. If some structural change takes place after the temperature drop from T_c to room temperature, the TEM information is not on the morphology developed at T_c but on that after the change. Real-time observation at T_c is desirable to discuss the kinetics of spherulite growth.

In this paper, we undertake real-time observation of morphology development in melt-crystallization of isotactic polypropylene (iPP) using a new light scattering photometer. The photometer facilitates the time-resolved analysis on morphology development in a time slice of 50 ms. iPP is known to form the spherulite of type A in Figure 1.[2] The objective of the work is to test scheme A by real-time observation.

Experimental Section

Materials and Measurement. Isotactic polypropylene (iPP) was supplied by Mitsui Toatsu Chemicals, Inc. (J3HG; $M_w = 3.5 \times 10^5$, $M_n = 5.0 \times 10^4$). The nucleating agent (NA) was 2,2-methylenebis(4,6-di-*tert*-butylphenyl) sodium phosphate (MARK NA-11) supplied by Asahi Denka Co., Ltd. NA was loaded to provide the dense nucleation which causes intensive scattering of light to facilitate the analysis of the early stage of crystallization by the light scattering method.

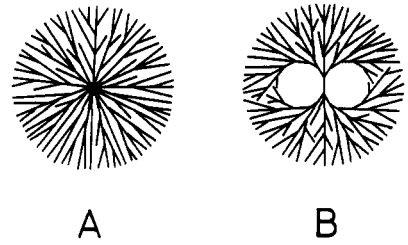

Figure 1. Cartoon of the two basic spherulite types: reproduced from ref 1.

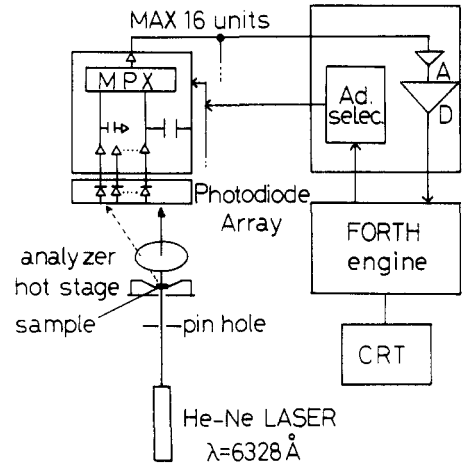

Figure 2. Light scattering apparatus.

iPP and NA (0.1 wt %) were mixed by a mixing extruder (CS-194, Custom Scientific Instrument, Inc.) at 200 °C, and the extrudate was chopped into pellets. A thin-layer specimen (ca. 40 μm thick) was prepared by pressing the pellets between two cover glasses at 200 °C.

After holding the specimen at 200 °C for 3 min, it was rapidly transferred into a light scattering hot-stage set at a crystallization temperature. Figure 2 shows the light scattering photometer with a 46-photodiode-array system which realizes the time-resolved measurement of an angular distribution of scattered light in a time slice of 50 ms.[3] The scattering measurements were carried out under both H_V (cross-polarized) and V_V (parallel-polarized) optical alignments.

Method of Analysis. When there is no azimuthal angle dependence, the angular distributions of V_V scattering intensity

* To whom correspondence should be addressed.

0024-9297/92/2225-1908$03.00/0

I_{V_V} and that of H_V scattering I_{H_V} are described as[4]

$$I_{V_V} - (4/3)I_{H_V} \propto \langle \eta^2 \rangle \int_0^\infty \gamma(r) \frac{\sin qr}{qr} 4\pi r^2 \, dr \quad (1)$$

$$I_{H_V} \propto \langle \delta^2 \rangle \int_0^\infty f(r) \frac{\sin qr}{qr} 4\pi r^2 \, dr \quad (2)$$

where $\langle \eta^2 \rangle$ is the mean-square density fluctuation, $\gamma(r)$ is the correlation function of the density fluctuation, q is the magnitude of the scattering vector, $\langle \delta^2 \rangle$ is the mean-square anisotropy, and $f(r)$ is the correlation function of the orientation fluctuation in an optical axis. At the early stage of crystallization, crystalline domains are usually isolated and their size and number increase with time so that eq 2 should be rewritten as

$$I_{H_V} \propto \langle \delta^2 \rangle \int_0^\infty [\phi_d + (1 - \phi_d)\gamma(r)] f(r) \frac{\sin qr}{qr} 4\pi r^2 \, dr \quad (3)$$

where ϕ_d is the volume fraction of the crystalline domain. At the early stage of crystallization, ϕ_d is close to 0 and eq 3 is approximated as

$$I_{H_V} \propto \langle \delta^2 \rangle \int_0^\infty \gamma(r) f(r) \frac{\sin qr}{qr} 4\pi r^2 \, dr \quad (4)$$

At the late stage, ϕ_d is close to 1 and eq 3 is reduced to eq 2.

To discuss the crystallization kinetics, it is convenient to define the integrated scattering intensities, invariants Q_η and Q_δ:

$$Q_\eta = \int_0^\infty (I_{V_V} - (4/3)I_{H_V}) q^2 \, dq \quad (5)$$

$$Q_\delta = \int_0^\infty I_{H_V} q^2 \, dq \quad (6)$$

By eqs 1, 3, 5, and 6, Q_η and Q_δ are given by[5]

$$Q_\eta \propto \langle \eta^2 \rangle = \phi_d(1 - \phi_d)(\alpha_d - \alpha_0)^2 \quad (7)$$

$$Q_\delta \propto \langle \delta^2 \rangle = \phi_d \delta_d^2 \quad (8)$$

$$\delta_d = \phi_c(\alpha_1 - \alpha_2) \quad (9)$$

where α_d is the average polarizability of the crystalline domain, α_0 is the polarizability of the melt, ϕ_c is the internal crystallinity of the crystalline domain, and α_1 and α_2 are the principal polarizabilities of the crystal lamella. Hence, from the time variation of $\langle \eta^2 \rangle$ ($\propto Q_\eta$) and $\langle \delta^2 \rangle$ ($\propto Q_\delta$), one can discuss the crystallization kinetics in terms of ϕ_d and ϕ_c as a function of time.

Results and Discussion

All specimens in this study showed circular-symmetric scattering patterns in both H_V and V_V modes; i.e., there was no azimuthal angular dependence. Both intensities I_{H_V} and $(I_{V_V} - (4/3)I_{H_V})$ decreased monotonously with the scattering angle. As typically shown, in Figure 3, the angular dependence was well described by the Debye–Bueche type scattering function[6,7]

$$I(q) = \left(\frac{1}{A + Bq^2} \right)^2 \quad (10)$$

where A and B are constants (the intercept and slope of Figure 3). By eqs 10 and 5 or 6, invariants Q_η and Q_δ are given by

$$Q_i = \pi / 4A(AB)^{1/2} \quad (11)$$

where $i = \eta$ and δ. The calculated Q_η ($\propto \langle \eta^2 \rangle$) and Q_δ ($\propto \langle \delta^2 \rangle$) at 128 °C are plotted as a function of the crystallization time in Figure 4. In Figure 4 $\langle \eta^2 \rangle$ starts to increase after an induction period, attains a maximum, and then decreases. By eq 7, the $\langle \eta^2 \rangle$ maximum occurs when ϕ_d attains 0.5; i.e., the crystalline domains grow and occupy 50% volume. It is a quite conceivable result for the spherulite growth. The time variation of $\langle \delta^2 \rangle$ is also conceivable for the spherulite growth in light of eq 8. However, the difference in the onset time between $\langle \eta^2 \rangle$ and $\langle \delta^2 \rangle$ is unexpected. That is, $\langle \eta^2 \rangle$ starts to increase at $t = t_0$, and then after a certain time lag, the onset of $\langle \delta^2 \rangle$ is seen at $t = t_1$. In contrast, by the current understanding of spherulite growth, one may expect a simultaneous onset of $\langle \eta^2 \rangle$ and $\langle \delta^2 \rangle$. The question is what happens during the time lag of $(t_1 - t_0)$.

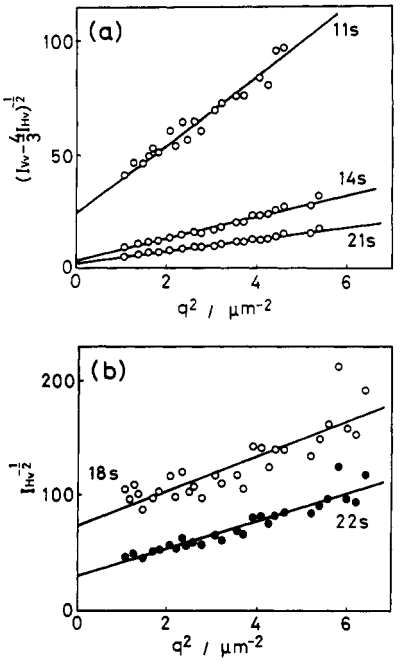

Figure 3. Debye–Bueche plot: (a) $I_{V_V} - (4/3)I_{H_V}$; (b) I_{H_V}.

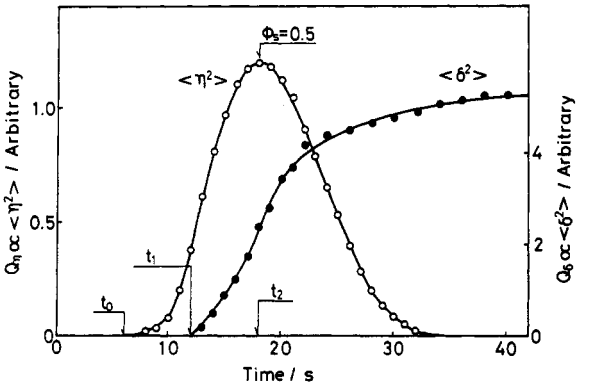

Figure 4. Time variations of the density ($\langle \eta^2 \rangle$) and orientation ($\langle \eta^2 \rangle$) fluctuations.

The time lag may be ascribed to the development of an isotropic embryo as the precursor of spherulite. However, what is the isotropic embryo? One may mention two possibilities: one is a high-density domain by the thermal fluctuation, and the other is a less-ordered crystalline domain. If the former is the case, $\langle \eta^2 \rangle$ and $\langle \delta^2 \rangle$ will show an abrupt increase when the high-density domain transformed to the crystalline domain, say, at $t = t_1$. The result in Figure 4 is against this; i.e., $\langle \eta^2 \rangle$ and $\langle \delta^2 \rangle$ increase continuously with time at the early stage. The latter possibility seems to be more realistic. It implies that one has to discuss the crystallization kinetics by taking account of the isotropic nature in early stages.

When ϕ_d is small, eq 7 is approximated as

$$Q_\eta \propto \phi_d \quad (12)$$

When the Avrami equation[8] is applied for the early stage, the time variation of ϕ_d is given by

$$\phi_d = 1 - \exp(-\beta(t - t_0)^\alpha) \quad (13a)$$

$$\phi_d \simeq \beta(t - t_0)^\alpha \quad (13b)$$

where α is the Avrami index and β is the overall crystallization rate constant given by

$$\beta \simeq \frac{\ln 2}{(\tau_{1/2,\eta})^\alpha} \quad (14)$$

where $\tau_{1/2,\eta}$ is the half-crystallization time. $\tau_{1/2,\eta}$ can be easily obtained by the scattering method, i.e., as a time difference between the maximum time t_2 and the onset time t_0 in Figure 4. Typical Avrami plots are shown in Figure 5. α is given by the slope of a straight line, and then the value of β is obtained.

When the isotropic embryo is spherical, its average radius $\bar{R}$ is given as a function of the Debye–Bueche correlation distance $a = (B/A)^{1/2}$ (see eq 10) and the volume fraction ϕ_d:

$$\bar{R} = 3a/4(1 - \phi_d) \quad (15)$$

By eqs 12–15, one can estimate the time variation of $\bar{R}$. The typical results are shown in Figure 6.

A linear growth of the isotropic embryo is seen in Figure 6, and then, from the slope, the growth rate G_η ($=d\bar{R}/dt$) is given. As discussed above, if the isotropic embryo is the less-ordered crystalline domain, its growth is expected to be governed by the crystallization kinetics, e.g., by the Hoffman–Lauritzen (H–L) theory.[9,10] The test will be achieved by investigating the temperature dependence of G_η as follows.

According to the H–L theory, the spherulite growth rate G is described by

$$G/\exp\left(-\frac{U}{R_g(T_c - T_\infty)}\right) \propto \exp\left(-\frac{K}{T_c \Delta T f}\right) \quad (16)$$

where R_g is the gas constant, ΔT ($=T_m^\circ - T_c$) is the supercooling, T_m° is the equilibrium melting temperature, T_c is the crystallization temperature, $T_\infty = T_g - 30$, T_g is the glass transition temperature, $U = 1500$ cal/mol, f is the correction factor given by $2T_c/(T_m^\circ + T_c)$, and K is the parameter which depends on the crystallization regime. The results of kinetic analysis on G_η are shown by closed circles in Figure 7. Here also shown by open circles are the similar results reproduced from the previous paper,[11] in which we obtained the growth rate G_{OM} by polarized microscopic observation. Note that G_{OM} was obtained for the growth of the crystalline domain identified definitely as the spherulite. Both temperature dependences of G_η and G_{OM} consist of two straight lines, suggesting that both kinetics follow the H–L theory and a regime transition from III (II) to II (III) takes place at the same temperature ($T_c = 140$ °C). Anyway, the isotropic embryo seems to have the crystalline nature.

Now, following the above scenario, the isotropic embryo exists at the early stage, and then it would grow up to the more ordered domain, such as the spherulite. The kinetical discussion should be extended to the intermediate and late stages.

Using eqs 8, 9, and 13a, a relative degree of crystallinity in the crystalline domain Φ_c may be described by

$$\Phi_c = \frac{\phi_c(t)}{\phi_c(\infty)} = \frac{\langle\delta^2\rangle_t^{1/2}}{\langle\delta^2\rangle_\infty^{1/2}[1 - \exp(-\beta(t - t_0)^\alpha)]^{1/2}} \quad (17)$$

where $\phi_c(\infty)$ is the attainable crystallinity in the crystalline domain (e.g., impinged spherulite) at a given crystallization condition. Typical time variations of Φ_c estimated by eq 17 are shown in Figure 8. The time axis is normalized by $\tau_{1/2,\eta}$. Φ_c is found to increase gradually with time. That is, the crystallization proceeds in the domain with its growth. Note that the isotropic regime before the onset of H_V scattering locates in a time range of $(t - t_0)/\tau_{1/2,\eta} < 0.4$ for various crystallization temperatures. The extrapolated values of Φ_c in the isotropic domain are small, suggesting a low crystallinity.

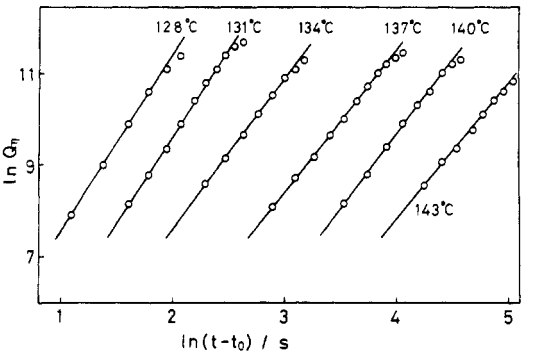

Figure 5. Avrami plots of $Q_\eta \propto \langle\eta^2\rangle$.

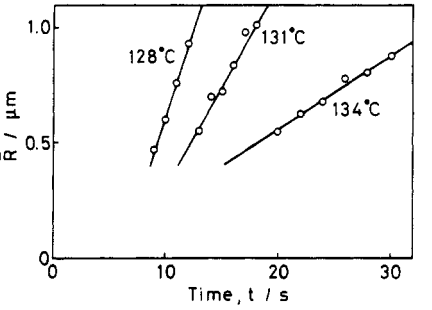

Figure 6. Time variation of the radius of the isotropic domain.

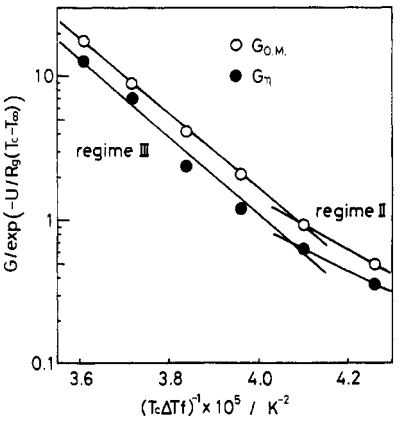

Figure 7. Temperature dependence of the growth rate of the isotropic domain (G_η) and that of the spherulite (G_{OM}; reproduced from ref 11).

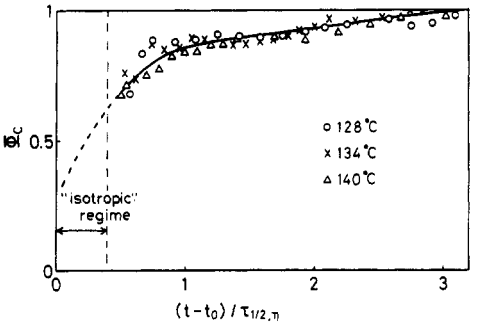

Figure 8. Time variation of the relative crystallinity Φ_c.

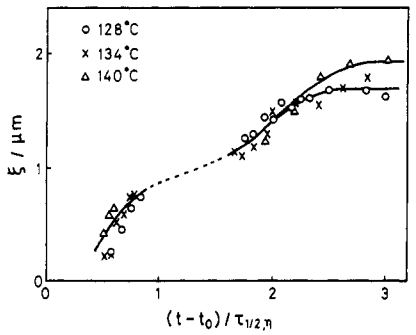

Figure 9. Time variation of the orientation correlation distance ξ.

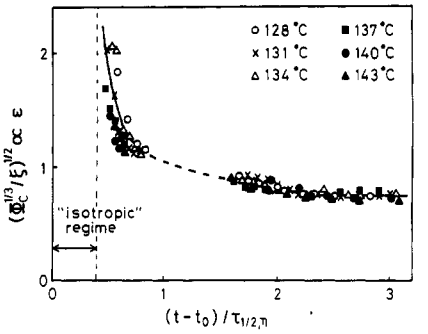

Figure 10. Time variation of the disorder parameter ϵ.

Thus the relative crystallinity seems to increase with time at the intermediate and late stages. Then the next problem to be discussed is the ordering process. The ordering can be analyzed in terms of scattering variables as follows.

By the random orientation correlation approximation,[4] the orientation correlation distance ξ is described by[12]

$$\xi = 2d/3\epsilon^2 \tag{18}$$

where d is the size of the fibril (consisting of lamellae) and ϵ is the average angle between the optical axis of a fibril and that of the nearest neighbor. ϵ is assumed to be a parameter describing the degree of disorder in fibrillar arrangement.[13] The value of ξ can be estimated by the scattering profiles, i.e., by the Debye–Bueche correlation distances a and b, both given by $(B/A)^{1/2}$ on the basis of eq 10, for the V_V and H_V scatterings, respectively

$$\xi = ab/(a - b) \tag{19}$$

for the early to intermediate stages ($\phi_d \sim 0$) and

$$\xi = b \tag{20}$$

for the late stage ($\phi_d \sim 1$).

The value of d in eq 18, on the other hand, can be estimated as

$$d \propto \Phi_c^{1/3} \tag{21}$$

since $\Phi_c = Nd^3/(N_\infty d_\infty^3)$, where N is the number of crystallites (stacked lamellae) in a crystalline domain and ∞ denotes the attainable (or final) stage of crystallization. Note that eq 21 is given by assuming that N does not vary with time, i.e., being constant, $N = N_\infty$. (The case of $N \neq N_\infty$ will be discussed later.) Consequently, the disorder parameter can be obtained by

$$\epsilon \propto (\Phi_c^{1/3}/\xi)^{1/2} \tag{22}$$

Typical time variations of ξ obtained by eqs 19 and 20 are shown in Figure 9. The orientation correlation distance is shown to increase with time at various crystallization temperatures. In Figure 10 are shown typical time variations of ϵ combining the results in Figures 8 and 9 on the basis of eq 22. At the early to intermediate stages, the disorder parameter is shown to decrease quite rapidly with time. Then, the decrease slows down and eventually ϵ remains constant at the very late stage.

So far, the analysis has been based on the assumption of constant N ($=N_\infty$) throughout the crystallization. If one employs a more realistic assumption that N increases with time to approach N_∞, e.g., $N \propto \Phi_c$, ϵ is easily shown to have a stronger time dependence than in Figure 10. In reality, both d and N may increase with time, yielding the similar time variation of ϵ as shown in Figure 10.

If one extrapolates the results in Figure 10 to the early stage, at which the H_V scattering has not been detected and hence ϵ cannot be defined, the ϵ values are expected to be very large. It implies that the crystalline arrangement is highly disordered in the isotropic domain. Further, recalling the similar argument in Figure 8 that the crystallinity Φ_c should be very low at the early stage, one may conclude that the isotropic domain is a crystalline one with low Φ_c and high ϵ. The disordered domain with a low crystallinity should look isotropic for the light so that it will render the time lag in Figure 4.

It is interesting to note that, even after the isotropic domain well grows up, say, to 0.5 μm in radius (see Figure 6), it is still highly disordered. It may be caused by the fast crystallization, yielding highly branched lamellae. Such a situation might be characteristic of the iPP, which is known to form the cross-hatched structure.[2,14] However, the presence of the isotropic precursor itself might be a more general phenomenon for the fast crystallization of bulk polymers. Time-resolved light scattering studies on the early stage of crystallization in various polymers is an interesting subject for future studies.

References and Notes

(1) Wunderlich, B. *Macromolecular Physics*; Academic Press: New York, 1973; Chapter 3.7.
(2) Norton, D. R.; Keller, A. *Polymer* **1985**, *26*, 704.
(3) Suehiro, S.; Sugimoto, K. *Nikkei Electron.* **1986**, No. 396, 213.
(4) Stein, R. S.; Wilson, P. R. *J. Appl. Phys.* **1962**, *33*, 1914.
(5) Koberstein, J.; Russell, T. P.; Stein, R. S. *J. Polym. Sci., Polym. Phys. Ed.* **1979**, *17*, 1719.
(6) Debye, P.; Bueche, A. M. *J. Appl. Phys.* **1949**, *20*, 518.
(7) Debye, P.; Anderson, H. R., Jr.; Brumberger, H. *J. Appl. Phys.* **1957**, *28*, 679.
(8) Avrami, M. J. *J. Chem. Phys.* **1939**, *7*, 1103.
(9) Lauritzen, J. I., Jr.; Hoffman, J. D. *J. Appl. Phys.* **1973**, *44*, 4340.
(10) Clark, E. J.; Hoffman, J. D. *Macromolecules* **1984**, *17*, 878.
(11) Okada, T.; Saito, H.; Inoue, T. *Macromolecules* **1990**, *23*, 3865.
(12) Stein, R. S.; Stidham, S. N. *J. Appl. Phys.* **1964**, *35*, 42.
(13) Stein, R. S.; Chu, W. *J. Polym. Sci., Polym. Phys. Ed.* **1970**, *8*, 1137.
(14) Sano, H.; Usami, T.; Nakagawa, H. *Polymer* **1986**, *27*, 1497.